Single-cell electroporation arrays with real-time monitoring and feedback control†

Michelle Khine,*[ab] Cristian Ionescu-Zanetti,[b] Andrew Blatz,[b] Lee-Ping Wang[b] and Luke P. Lee[c]

Received 3rd October 2006, Accepted 7th February 2007
First published as an Advance Article on the web 7th March 2007
DOI: 10.1039/b614356c

Rapid well-controlled intracellular delivery of drug compounds, RNA, or DNA into a cell – without permanent damage to the cell – is a pervasive challenge in basic cell biology research, drug discovery, and gene delivery. To address this challenge, we have developed a bench-top system comprised of a control interface, that mates to disposable 96-well-formatted microfluidic devices, enabling the individual manipulation, electroporation and real-time monitoring of each cell in suspension. This is the first demonstrated real-time feedback-controlled electroporation of an array of single-cells. Our computer program automatically detects electroporation events and subsequently releases the electric field, precluding continued field-induced damage of the cell, to allow for membrane resealing. Using this novel set-up, we demonstrate the reliable electroporation of an array (n = 15) of individual cells in suspension, using low applied electric fields (<1 V) and the rapid and localized intracellular delivery of otherwise impermeable compounds (Calcein and Orange Green Dextran). Such multiplexed electrical and optical measurements as a function of time are not attainable with typical electroporation setups. This system, which mounts on an inverted microscope, obviates many issues typically associated with prototypical microfluidic chip setups and, more importantly, offers well-controlled and reproducible parallel pressure and electrical application to individual cells for repeatability.

Introduction

Quantitative data from a large number of individual cells provide a wealth of information and insight typically obscured by bulk measurements. Bulk population experiments output the mean value of a parameter of interest, whereas single-cell experiments allow for investigating the distribution of that parameter.[1] This is an important distinction because even cells that are identical genetically exhibit marked variations in gene expression and behavior.[2] Information on a cell's time- or stimulus-dependent gene expression is lost when the sample's specific signal is diluted with those from surrounding cells, which do not exhibit the same expression. Heterogeneity in behavior across single-cells, observable even when the populations' behavior is reproducible and predictable, suggests that it cannot be deterministically described.[3]

Specifically examining the response of the cell to applied stimuli—at the single-cell level—offers a means to resolve and understand heterogeneity in cell behavior. Single-cell electroporation,[4–9] in which transient pores can be induced in a cell's membrane, when the transmembrane potential exceeds the dielectric breakdown voltage of the membrane (0.2–1.0 V),[10,11] offers several additional advantages over the more conventional bulk approach. Bulk electroporation (see ref. 12–15) in which millions of cells in suspension are subjected to high applied voltages (typically kV) in order to achieve the requisite transmembrane potential, has inherent drawbacks, which include joule heating, uncontrolled and non-homogenous field drops across the different cells, and as a consequence, a low percentage of viable, electroporated cells. Therefore, delivering a homogenous dose of exogenous compounds into all the cells is not possible. Reversible electroporation, in which the cell membrane reseals after release from the electric field, is also difficult.[16]

For successful single-cell electroporation, the cell should either be isolated or the electric field focused to target a particular cell.[17] This has been traditionally executed using glass patch micropipettes.[7,8,18] These studies do not monitor the current through the electroporation electrodes, and therefore do not output detailed measurements of current changes during poration. Rystten *et al.* addresses this by characterizing the time course of electroporation and resealing by using a patch-clamp pipette positioned at a 90° angle to the electroporation electrodes.[19] These aforementioned approaches have the inherent practical limitation, however, of being a serial process of addressing only one cell at a time.

Microfabricated devices are ideally and practically suited to both isolate single-cells and focus the electric field for reversible single-cell electroporation. In 2000, Huang *et al.* introduced the first microfabricated single-cell electroporation chip.[6] They developed a vertically stacked device with two microfabricated silicon substrates bonded together with a glass cover slip. A micro-hole etched through the nitride membrane connects the fluid chambers and the electroporation electrode. A single-cell is flowed-through, captured in the micro-hole by a pressure difference, electroporated, uploaded with exogenous

[a]*School of Engineering, University of California, Merced, USA. E-mail: mkhine@ucmerced.edu*
[b]*Fluxion Biosciences, Inc., San Francisco, CA 94158, USA*
[c]*Department of Bioengineering, University of California, Berkeley, USA*
† The HTML version of this article has been enhanced with additional colour images.

compounds, and released to be replaced by the next cell. In theory, this technology should be arrayable for multiple parallel measurements, but this has not yet been demonstrated.

Our approach differs significantly from existing technology. We first demonstrated our low-voltage elastomeric single-cell electroporation chip in 2005 which utilizes a simple, cost-effective and fast batch manufacturing approach.[9] Instead of a multilayered silicon device that requires precise two-side alignment, wafer bonding, and etching, we use a simple micromolding procedure to fabricate PDMS (polydimethylsiloxane) devices. Whereas the Huang *et al.* device cells are consecutively addressed, we have an array such that a plurality of cells can be simultaneously sequestered and electroporated. A next batch of cells can then be moved in and porated. In the same amount of time it takes to manipulate one cell in the flow-through design, we can manipulate an array of cells. Moreover, in our design, we can monitor several cells side by side in the same field of view for comparison (Fig. 1).

This lateral trapping approach allows trapped cells to be arrayed with a distance as close as 20 μm, increasing the cell density in the active area of the device by two orders of magnitude over existing microfabricated electroporation set-ups. Additionally, using our lateral cell trapping geometry, the cell's deformation into the trapping capillary is in the same horizontal optical plane as the cell body. Therefore, the entry of compounds from the locally electroporated portion into the cell body can be easily visualized *via* fluorescence microscopy. We mated our microfluidic electroporation devices to standard 96-well plates such that compounds and cells can be easily introduced. The transparent elastomer PDMS, unlike opaque silicon, enables fluorescent detection and monitoring throughout the whole process.

Compared to glass micropipette experiments, this set-up does not require manipulation of pipettes, vibration isolation equipment, high voltages, or adherent cells. We also use Ag/AgCl electrodes and a patch clamp amplifier, allowing accurate current traces not commonly reported. In traditional electroporation set-ups (with large parallel electrodes), the bulk of the current is carried by the extracellular electrolyte solution, making it impossible to record the current through a single-cell. Therefore, Hibino *et al.* used voltage sensitive dyes (RH 292) to examine the time course of bulk electroporation with submicrosecond resolution, to estimate membrane resistance and membrane capacitance.[20]

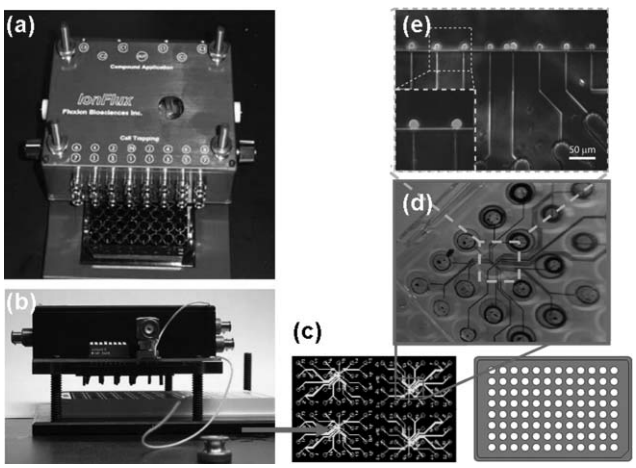

Fig. 1 The bench-top setup: (a) top view of interface which mates by pressure fit to a 96-well bottomless-plate, which mates to the microfluidic chips; (b) side view showing the hollow Ag/AgCl electrodes dipping into the wells; (c) schematic of chips mapped to the bottom of a plate (right); (d) bottom of plate showing one of the devices; (e) viewing window (within one of the wells) of an array of HeLa cells trapped (overlay of bright field and FITC).

In contrast to these approaches, we concentrate on the analysis of changes in cell membrane resistance due to electroporation, by directly measuring current jumps due to membrane poration in a single-cell, and continuously monitoring resistance thereafter. We first demonstrated this in 2005,[9] and the validity of this approach has been recently demonstrated using glass pipettes by Krassen *et al.*[21] Using this, we now demonstrate real-time feedback control of electroporation conditions such that the parameters do not need to be determined empirically *a priori*. We apply a homogenous electric field across a small portion of the cell membrane that is locally electroporated such that we can controllably dose individual cells with exogenous compounds.

Methods and materials

1. Electroporation device

The mold for the PDMS device is fabricated using a photolithography process as previously described.[9,22] The PDMS microfluidic devices are then bonded to a bottom-less, standard 96-well plate (Nalge Nunc International) using a plasma treatment (Fig. 1). The 96-well plate is divided into four (4 × 6) quadrants. Within each quadrant, one viewing window (within one of the wells) contains all the trapping sites. As such, all of the trapped cells are within one field of view of the microscope. The anodized aluminium enclosure serves as an effective faraday cage for low noise recordings (Fig. 1). The device is loaded using standard pipettes, with cells and compounds loaded into the wells before placing the plate-chip assembly into the pressure interface. Each of the wells (with the exception of the viewing window) has a hollow Ag/AgCl electrode for pressure and electrical connection to individually addressable microfluidic channels within the chip. The electrodes are connected to a printed circuit board (PCB) for electrical output within the interface. The interface was designed to fit easily into existing equipment, such as inverted microscopes and patch clamp amplifiers. As such, the interface has a universal connector to any amplifier's head-stage (in this setup, the Warner 505B Patch Clamp Amplifier) for voltage application and current recording. The electronics are controlled with a custom graphical user-interface (National Instruments, LabView 6.0) and data acquisition performed *via* a data acquisition card (PCI-6024E, National Instruments). Switching from one channel to the next (for 15 channels) is manual (eliminating the switching noise associated with on-board multiplexing) and uses a rotary dial on the side of the interface box.

A pressure-control box was also developed to attach to the pressure box of the interface *via* Luer connectors. The channels could thus be configured to trap all the cells simultaneously or individually, with a range of positive and negative applications

from −381 mm Hg to 381 mm Hg. An optimal cell trapping pressure was used such that the cells trap rapidly, and yet are not damaged by excessive pressure.

2. Computer algorithm

The computer program is written in LabView 6.0, a visual programming language by National Instruments. Voltage pulse lengths are user defined. Square waves from 0 to 1.0 V are applied in 0.1 V increments until electroporation occurs. For these experiments, we defined the threshold for electroporation to be when the slope of the current changes by more than 150% (the current before electroporation, *i.e.*, leak current, is linear). This electroporation criteria is tunable, and can be user defined. We implemented a control loop to immediately terminate application of voltage after electroporation. Therefore, the next increment of voltage application would be prevented. Following electroporation, a small voltage (20 mV) is applied at a frequency rate of 10 kHz in order to monitor resealing kinetics.

3. Experimental procedure

One quadrant (with one device) of the 96-well plate-chip assembly is used per experiment. Prior to loading, the plate-chip assembly is placed in a vacuum chamber to create negative pressure within the chip's microchannels to facilitate easier loading (buffer solution without cells). 270 μL of solution (cells or compounds) are then pipetted into each of the 24 wells, with the exception of the viewing window. This volume is required to ensure electrical connection with the electrodes that dip into the wells. The 96-well plate assembly is then loaded into the aluminium interface. Screws on the interface are tightened for a pressure seal (Fig. 1). Human cervical cancer HeLa cells, cultured in Dulbecco's Modified Eagle Medium (Gibco) with 10% fetal bovine serum until 90% confluency, are first harvested by incubation with trypsin (Invitrogen) for 3 min and suspended in carbon dioxide independent medium (Invitrogen) with 10% fetal bovine serum to neutralize the trypsin. The suspension is then centrifuged and resuspended in Dulbecco's phosphate buffered saline (PBS, Gibco). Cells were flown in and trapped with a slight negative pressure (−127 mm Hg). Electroporation was tested with both a sustained holding pressure on the cells, and with the pressure released. The voltage is applied between an electrode that connects to an individual cell trapping channel and one that connects to the main channel. The chip is optically monitored with an inverted microscope (Eclipse TS100, Nikon) using a fluorescent module, and is video captured with a camera (Cascade 512B) and a video capture card (microVideo DC50, Pinnacle) on the same computer. The whole process is video captured at a sampling rate of 30 fps.

Results

To determine optimal electroporation conditions, we tested various pulse parameter lengths (5 ms, 10 ms, 30 ms and 60 ms) with a voltage step size of 0.1 V from 0 V to 1.0 V (Fig. 2). At shorter pulse widths, higher voltages are required to achieve electroporation (Fig. 3a). The characteristic jump in current is

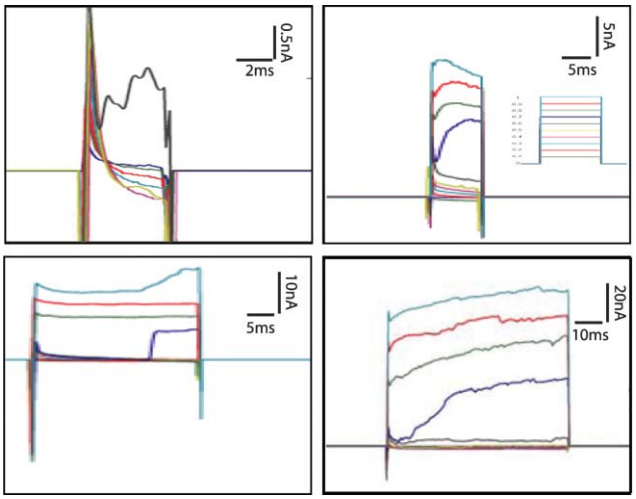

Fig. 2 Typical current *versus* time graphs. Current is measured in response to applied square wave voltages (inset) of varying durations, for 5 ms, 10 ms, 30 ms, and 60 ms respectively (clockwise from top left).

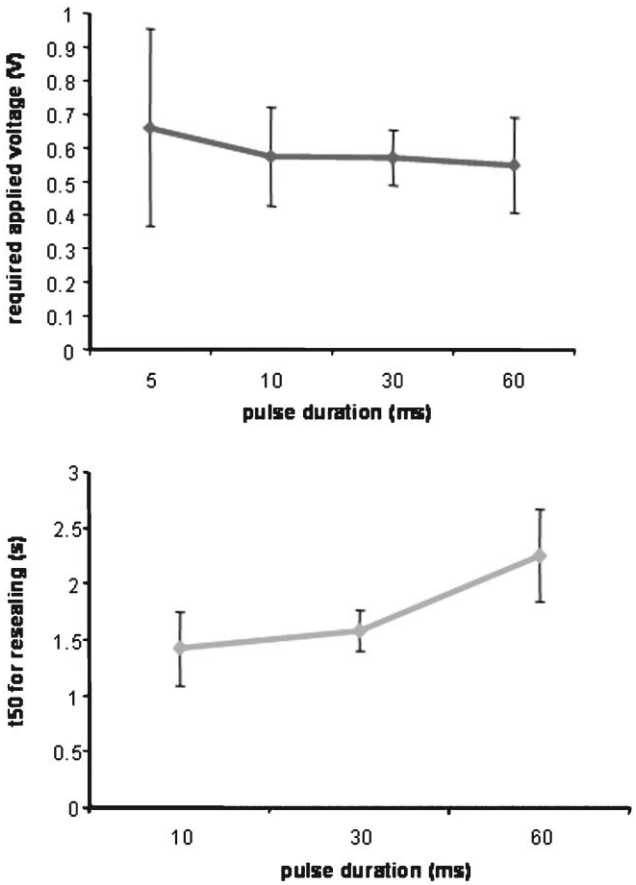

Fig. 3 Resealing as a function of pulse conditions. The voltage required to achieve electroporation (top) and the resealing time (bottom) are plotted as a function of pulse duration. Shorter pulses typically require higher voltages, but biological cell-to-cell viability is evident. The time required to achieve 50% resealing is shown as an indication of resealing timescale.

indicative of pores opening as ions are allowed to pass. The leak current is linear and constant and, as such, is subtracted out. The open channel resistance ranges from 12–20 MΩ and the seal resistance for the cells were in the range of 40–70 MΩ.

While shorter pulse widths result in better resealing, achieving consistent and reproducible electroporation events at shorter pulse widths is more difficult (Fig. 3). For example, the standard error of the mean for required applied voltage at 5 ms, is large compared to the other pulse widths. At 5 ms and, to a lesser degree 10 ms, the cell does not electroporate on initial pulse application (subsequent pulse applications is sometimes required). At 30 ms and 60 ms, electroporation is consistent. Resealing is defined as the resumption of high resistance due to the closing of the pores, as determined by impedance. By applying a low amplitude square wave (20 mV) to measure the resistance immediately after the applied electroporation protocol, resealing kinetics can be resolved (Fig. 4 and Fig. 5b). Such time resolution of resistance monitoring was not previously attainable with other electroporation setups. From this, we can determine resealing time constants for various pulse conditions (Fig. 4).

The resealing time constant was defined as the time needed for the resistance to return to at least 50% of the original resistance. This is the time to achieve 50% of the difference between the initial and final resealing percentage. Example data and time domain fits are shown in Fig. 4 and the correlation between the pulse duration and t_{50} to resealing is shown in Fig. 3b. Longer pulse widths, as expected, require longer times for the cells to reseal on average. The average resealing time for 3 different pulse conditions is shown in Fig. 3b. These are within range of resealing times reported in the literature.[23–25]

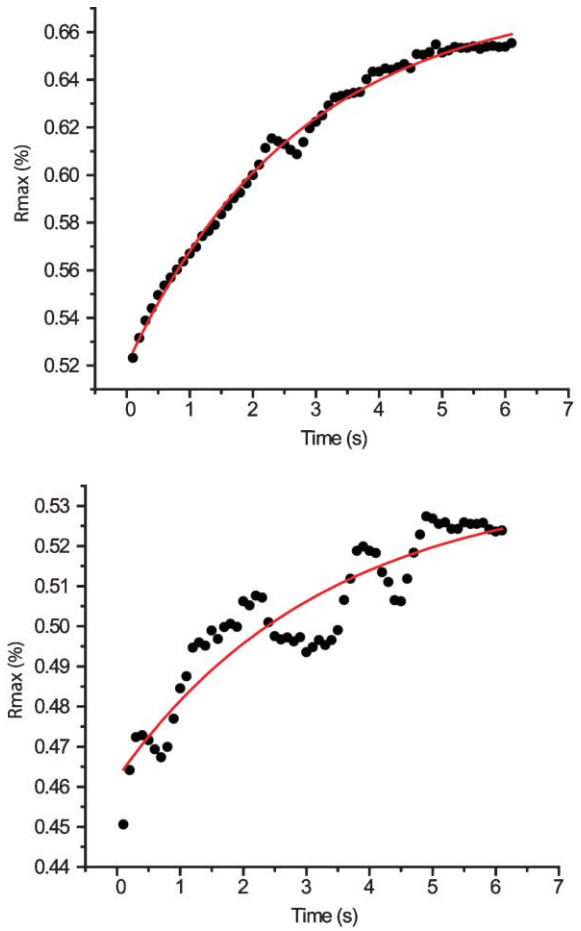

Fig. 4 Resealing kinetics for two cells. By fitting to an exponential, the time constant for 50% resealing (t_{50}) was determined. The average time constant is 1.75 s.

We also developed a graphical user-interface program that automatically releases the electric field when an electroporation event has occurred. The benefits of this automatic field shut-off is illustrated in Fig. 6, in which the same cell was electroporated without the control loop 4 times, and then electroporated 4 times with the control loop (intensity renormalized after each subsequent run). As is apparent from the graph, resealing kinetics improve dramatically when the feedback loop is used. With the control loop, we can electroporate a single-cell many times, with membrane resistance going back up after every electroporation event. For example, we have demonstrated electroporation of the same cell 9 times (as shown in Fig. 6).

Discussion

We demonstrate the use of patch clamp amplifiers to effectively perform membrane resistance measurements before, during, and after electroporation events. This allows for the real-time detection of electroporation events, and monitoring of resealing kinetics. Using this approach, different pulse parameters were evaluated for resealability (Fig. 5b).

Most importantly, this approach gives us the possibility to detect electroporation events in real time and to terminate the application of subsequent voltage pulses after the membrane has been permeabilized (which would result in further damage to the cell membrane). This approach is shown to decrease the resealing time, and increase the membrane resistance after resealing has occurred. This approach establishes a technique for real-time control over electroporation parameters, and feedback from each cell's characteristic membrane breakdown event.

While our aim was to electroporate as gently as possible for improved resealing, we needed to balance this against the issue of keeping the pores open long enough such that impermeable exogenous compounds can diffuse in post-electroporation. This becomes a non-trivial problem when the pores reseal faster than the compounds can reach the cells. We initially tried to load compounds from the pre-loaded trapping channel using diffusion alone, but it apparently took considerably longer for Calcein dye (Invitrogen, MW = 622) to load *via* diffusion than the measured pore resealing time. Therefore, multiple electroporation events had to be used in order to demonstrate effective loading. Orange Green Dextran (OGD, Invitrogen, MW = 70 000 kD) was even more difficult to load by diffusion. The time for the dye to enter the cell does not correlate well with the resealing time. It must be noted that for the diffusion dye experiments in which loading was achieved, the control loop was not used.

In order to expedite compound introduction before the pores reseal, we have since augmented compound delivery

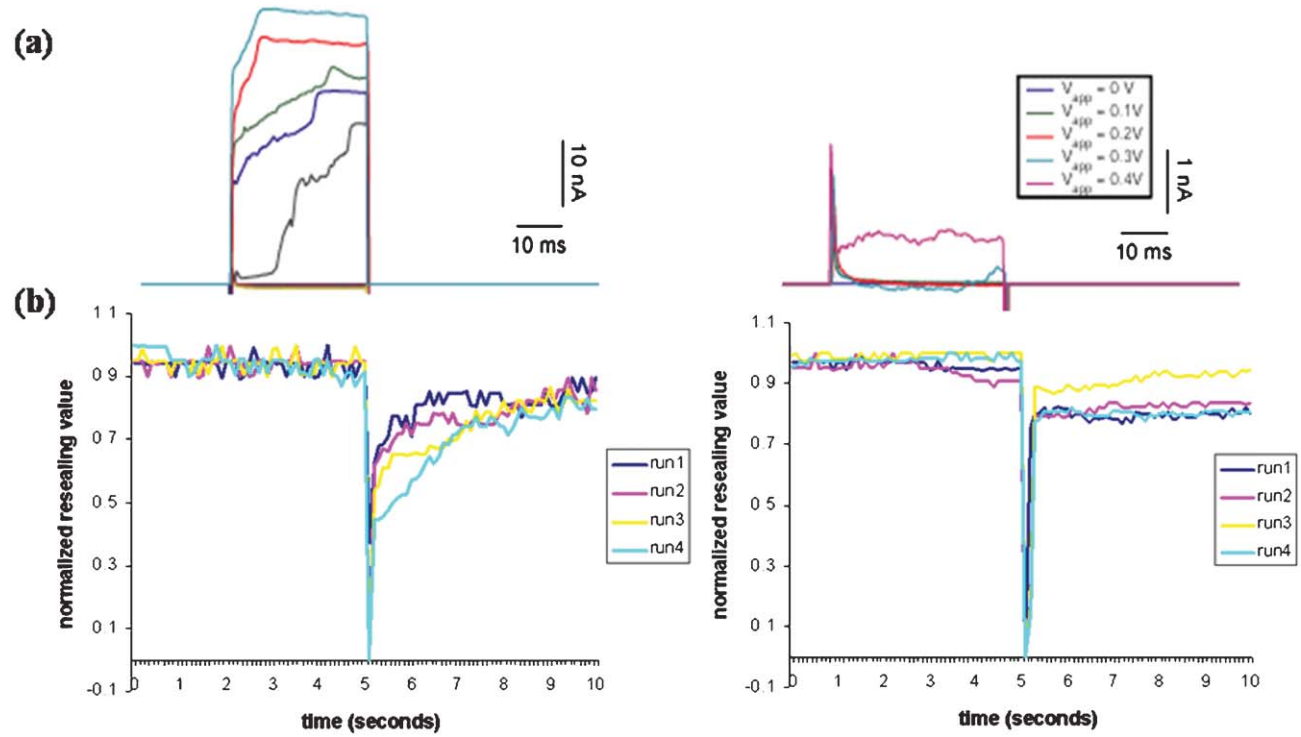

Fig. 5 Effects of the control loop: (a) example of current traces without the control loop (left) *versus* with control loop (right); (b) resealing after electroporation of a cell without control loop 4 times (left) *versus* resealing after electroporation of the same cell with the control loop (right).

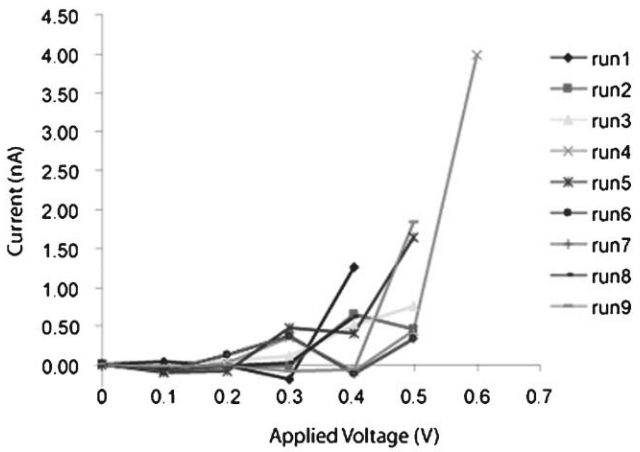

Fig. 6 Controlled electroporation. *I-V* curve for a single-cell electroporated 9 times with control loop.

using electrophoresis. A sustained low intensity electric field can be used to pre-concentrate the molecules of interest in the vicinity of the cell. While holding the cell, a constant negative voltage immediately after electroporation drives the compound into the cell. Using this methodology, Calcein was loaded into the cell within 3 s, whereas by diffusion alone it took upwards of 30 s. The intensity eventually plateaus, we suspect due to the pores resealing. Likewise, with the same applied voltage, OGD was loaded in the cell within a 60 s time span using the electrophoretic driving force (manuscript in preparation).

It must be noted, finally, that the resumption in conductance upon resealing may be due, at least in part, to the restoring of the seal between the aperture and the membrane. We do not yet have the means of delineating the effects of the pores resealing from the resealing of the cell to the channel.

Conclusions

In summary, we have developed a bench-top system comprised of a control interface, with mating disposable 96-well-formatted microfluidic chips, that enables cells to each be manipulated and monitored individually. This system can: (1) electroporate an array of single-cells using very low applied voltages (0.4–0.8 V); (2) automatically detect electroporation events; (3) monitor the cell's resistance before, during, and after electroporation; (4) ensure that the cell reseals in a timely manner; (5) reversibly electroporate the same cell multiple times; and (6) introduce membrane-impermeant compounds into the cytoplasm. We developed an automated computer algorithm so that electroporation conditions can be tailored to the response of individual cells, and need not be constant and pre-determined across the cell population. Such control enables us to electroporate all the cells, whereas in bulk approaches, only a portion of the cells are electroporated. Moreover, with this approach, it is possible to achieve controlled dosing not possible with bulk approaches. Using the developed software with feedback control, the electric field is removed immediately after electroporation which allows multiple electroporation events without irreversible damage to the cell. To the best of our knowledge, this is the first demonstration of feedback controlled electroporation of an array of single-cells.

Acknowledgements

Funding source: National Institute of Health NIGMS 1 R43 GM075509-01.

References

1 D. DiCarlo, N. Aghdam and L. P. Lee, Single-cell enzyme concentrations, kinetics, and inhibition analysis using high density hydrodynamic cell isolation arrays, *Anal. Chem.*, 2006, **78**, 4925–4930.
2 C. V. Rao, D. M. Wolf and A. P. Arkin, Control, exploitation and tolerance of intracellular noise, *Nature*, 2002, **420**, 231–237.
3 M. S. Ko, H. Nakauchi and N. Takahashi, The dose dependence of glucocorticoid-inducible gene expression results from changes in the number of transcriptionally active templates, *EMBO J.*, 1990, **9**, 2835–2842.
4 J. A. Lundqvist, F. Sahlin, M. A. I. Aberg, A. Stromberg, P. S. Eriksson and O. Orwar, Altering the biochemical state of individual cultured cells and organelles with ultramicroelectrodes, *Proc. Natl. Acad. Sci. U. S. A.*, 1998, **95**, 10356–10360.
5 K. Nolkrantz, C. Farre, A. Brederlau, R. I. D. Karlsson, C. Brennan, P. S. Eriksson, S. G. Weber, M. Sandberg and O. Orwar, Electroporation of Single Cells and Tissues with an Electrolyte-filled Capillary, *Anal. Chem.*, 2001, **73**, 4469–4477.
6 Y. Huang and B. Rubinsky, Micro-electroporation: improving the efficiency and understanding of electrical permeabilisation of cells, *Biomed. Microdevices*, 2000, **3**, 145–150.
7 K. Haas, W. C. Sin, A. Javaherian, Z. Li and H. T. Cline, Single-cell electroporation for gene transfer in vivo, *Neuron*, 2000, **29**, 583–591.
8 J. L. Rae and R. A. Levis, Single-cell electroporation, *Pflugers Arch.*, 2002, **443**, 664–670.
9 M. Khine, A. D. Lau, C. Ionescu-Zanetti, J. Seo and L. P. Lee, A Single Cell Electroporation Chip, *Lab Chip*, 2005, **5**, 38–43.
10 J. C. Weaver, Electroporation: a general phenomenon for manipulating cells and tissues, *J. Cell. Biochem.*, 1993, **51**, 426–435.
11 J. Teissie and M.-P. Rols, An experimental evaluation of the critical potential difference inducing cell membrane electropermeabilization, *Biophys. J.*, **65**, 409–413.
12 E. Neumann, M. Schaefer-Ridder, Y. Wang and P. H. Hofschneider, Gene transfer into mouse lyoma cells by electroporation in high electric fields, *EMBO J.*, 1982, **1**, 841–845.
13 Q. A. Zheng and D. C. Chang, High-efficiency gene transfection by in-situ electroporation of cultured cells, *Biochim. Biophys. Acta*, 1982, **1088**, 104–10.
14 T. Y. Tsong, Electroporation of cell membranes, *Biophys. J.*, 1991, **60**, 297–306.
15 J. C. Weaver and Y. A. Chizmadzhev, Theory of electroporation: A review, *Bioelectrochem. Bioenerg.*, 1996, **41**, 135–160.
16 D. C. Chang, B. M. Chassy, J. A. Saunders and A. E. Sowers, *Guide to Electroporation and Electrofusion*, Academic Press Inc., San Diego, 1992.
17 K. Nolkrantz, C. Farre, K. J. Hurtig, P. Rylander and O. Orwar, Functional Screening of Intracellular Proteins in Single Cells and in Patterned Cell Arrays Using Electroporation, *Anal. Chem.*, 2002, **74**, 4300–4305.
18 J. Olofsson, K. Nolkrantz, F. Rysttsen, B. Lambie, S. Weber and O. Orwar, Single-cell electroporation, *Curr. Opin. Biotechnol.*, 2003, **14**, 29–34.
19 F. Ryttsén, C. Farre, C. Brennan, S. G. Weber, K. Nolkrantz, K. Jardemark, D. T. Chiu and O. Orwar, Characterization of single-cell electroporation by using patch clamp and fluorescence microscopy, *Biophys. J.*, 2000, **79**, 1993–2001.
20 M. Hibino, H. Itoh and K. Kinosita, Jr., Time courses of cell electroporation as revealed by submicrosecond imaging of transmembrane potential, *Biophys. J.*, 1993, **64**, 1789–800.
21 H. Krassen, U. Pliquett and E. Neumann, Nonlinear current–voltage relationship of the plasma membrane of single CHO cells, *Bioelectrochemistry*, 2007, **70**, 71–77.
22 J. Seo, C. Ionescu-Zanetti, J. Diamond, R. La and L. P. Lee, Integrated multiple patch-clamp array chip via lateral cell trapping junctions, *Appl. Phys. Lett.*, 2004, **84**, 1973–1975.
23 E. Neumann, K. Toensing, S. Kakorin, P. Budde and J. Frey, Mechanism of electroporative dye uptake by mouse b cells, *Biophys. J.*, 1998, **74**, 98–108.
24 K. Kinosita, Jr. and T. Y. Tsong, Formation and resealing of pores of controlled sizes in human erythrocyte membrane, *Nature*, 1977, **268**, 438–441.
25 M. N. Teruel and T. Meyer, Electroporation-induced formation of individual calcium entry sites in the cell body and processes of adherent cells, *Biophys. J.*, 1997, **73**, 1785–1796.

